AFRL-IF-RS-TR-1998-184
Final Technical Report
September 1998


# MULTI-CHANNEL SIGNAL GENERATION AND ANALYSIS

**Research Associates for Defense Conversion, Inc.**

**Braham Himed**

*APPROVED FOR PUBLIC RELEASE; DISTRIBUTION UNLIMITED.*



**AIR FORCE RESEARCH LABORATORY**
**INFORMATION DIRECTORATE**
**ROME RESEARCH SITE**
**ROME, NEW YORK**

This report has been reviewed by the Air Force Research Laboratory, Information Directorate, Public Affairs Office (IFOIPA) and is releasable to the National Technical Information Service (NTIS). At NTIS it will be releasable to the general public, including foreign nations.

AFRL-IF-RS-TR-1998-184 has been reviewed and is approved for publication.

APPROVED:

DAVID D. FERRIS, JR.
Project Engineer

FOR THE DIRECTOR:

JOSEPH CAMERA, Deputy Chief
Information & Intelligence Exploitation Division
Information Directorate

If your address has changed or if you wish to be removed from the Air Force Research Laboratory Rome Research Site mailing list, or if the addressee is no longer employed by your organization, please notify AFRL/IFEA, 32 Brooks Road, Rome, NY 13441-4505. This will assist us in maintaining a current mailing list.

Do not return copies of this report unless contractual obligations or notices on a specific document require that it be returned.

# REPORT DOCUMENTATION PAGE

*Form Approved*
*OMB No. 0704-0188*



| 1. AGENCY USE ONLY *(Leave blank)* | 2. REPORT DATE | 3. REPORT TYPE AND DATES COVERED |
|---|---|---|
| | September 1998 | Final Sep 95 - Apr 96 |

**4. TITLE AND SUBTITLE**

MULTI-CHANNEL SIGNAL GENERATION AND ANALYSIS

**5. FUNDING NUMBERS**

C - F30602-95-C-0121, CLIN 0004
PE - 62702F
PR - 2304
TA - E8
WU - PE

**6. AUTHOR(S)**

Braham Himed

**7. PERFORMING ORGANIZATION NAME(S) AND ADDRESS(ES)**

Research Associates For Defense Conversion Inc.
10002 Hillside Terrace
Marcy NY 13403

**8. PERFORMING ORGANIZATION REPORT NUMBER**

N/A

**9. SPONSORING/MONITORING AGENCY NAME(S) AND ADDRESS(ES)**

AFRL/IFEA
32 Brooks Road
Rome NY 13441-4505

**10. SPONSORING/MONITORING AGENCY REPORT NUMBER**

AFRL-IF-RS-TR-1998-184

**11. SUPPLEMENTARY NOTES**

Air Force Research Laboratory Project Engineer: David Ferris/IFEA/(315) 330-4408

**12a. DISTRIBUTION AVAILABILITY STATEMENT**

Approved for public release; distribution unlimited.

**12b. DISTRIBUTION CODE**

**13. ABSTRACT** *(Maximum 200 words)*

This report documents the development, implementation and evaluation of signal generation and processing techniques oriented towards improving the detection and estimation of targets and other parameters in noisy and cluttered environments. It also attempts to quantify improvements in the detection and estimation of targets in noisy and cluttered environments.

Three methods for signal generation are discussed in the report. The first is referred to as a physical model signal generation. The second technique describes the representative model. The third technique is hybrid generated from both previously described technique.

**14. SUBJECT TERMS**

Physical Model, Representative Model, Hybrid Model, Signal Generation

**15. NUMBER OF PAGES**

54

**16. PRICE CODE**

| 17. SECURITY CLASSIFICATION OF REPORT | 18. SECURITY CLASSIFICATION OF THIS PAGE | 19. SECURITY CLASSIFICATION OF ABSTRACT | 20. LIMITATION OF ABSTRACT |
|---|---|---|---|
| UNCLASSIFIED | UNCLASSIFIED | UNCLASSIFIED | UL |

# Table of Content

# List of Figures

## Definitions of Variables

$d$ : Element spacing
$\lambda_c$ : Transmitter wavelength
$\phi_0$ : Mainbeam clutter return azimuth angle
$\phi_P$ : Azimuth angle to the p-th cell
$\phi_t$ : Target azimuth angle
$\phi_i$ : Interference azimuth angle
$\theta_0$ : Mainbeam clutter return elevation angle
$\theta_P$ : Elevation angle to the p-th cell
$\theta_t$ : Target elevation angle
$\theta_i$ : Interference elevation angle
$f_p$ : Doppler frequency of the p-th clutter cell
$f_t$ : Target Doppler frequency
$f_i$ : Interference Doppler frequency
$\varpi_p$ : Normalized Doppler frequency of the p-th clutter cell
$\varpi_t$ : Normalized target Doppler frequency
$\varpi_i$ : Normalized interference Doppler frequency
$\vartheta_p$ : Normalized spatial frequency of the p-th clutter cell
$\vartheta_t$ : Normalized target spatial frequency
$\vartheta_i$ : Normalized interference spatial frequency
$v_p$ : Platform velocity
$v_t$ : Target velocity
$v_I$ : Interference velocity
$\delta_0$ : Initial signal phase angle
$\gamma$ : Crab angle
$f_{PRF}$ : Pulse repetition frequency
$T$ : Pulse period
$\Delta\phi$ : Clutter patch angular extent
$N_c$ : Number of clutter patches in a clutter ring
$\gamma_c$ : Surface clutter reflectivity model parameter
$r_{c0}$ : Range to the primary clutter ring
$\Delta r_R$ : Radar range resolution
$\Delta r_p$ : Clutter patch range extent
$\psi_c$ : Clutter ring grazing angle
$\upsilon$ : Clutter ridge slope in the Doppler and spatial frequency domain
$v$ : Velocity of light

$G_0$ : Transmit pattern gain

$G_B$ : Array element backlobe pattern gain

$L_S$ : System losses

$T_U$ : Uncompressed pulse duration

$\lambda_T$ : Threshold

# 1

# Introduction

The objective of this effort is to develop, implement and evaluate signal generation and processing techniques oriented towards improving the detection and estimation of targets and other parameters in noisy and cluttered environments. It is also desired to quantify any improvements in the detection and estimation of targets in noisy and cluttered environments.

In developing new or enhancing existing signal processing algorithms for improved detection and estimation performance of exiting and planned sensors, one has to be aware of environmental induced effects and how the algorithm optimizes the sensor performance. In many cases, optimization is achieved by generating a set of weights and then applying them to the elements of both array elements and time delay elements of the system. Space Time Adaptive Processing (STAP) is one example of these adaptive processes. Performance evaluation and a fair comparative analysis of these techniques require the developer/user to have a signal generation that is compatible with real world data. However, modeling these effects is a very tedious and difficult task. For these reasons, alternative approaches to the physical model signal generation are sought. This will speed up analyses. Furthermore Monte Carlo type analyses can be done in a timely manner. The "representative model" that was suggested by Dr. James Michels of the Air Force Research Laboratory (AFRL), Sensor Directorate (SNRT) is one such example [1].

In this effort, we discuss three methods for signal generation. First, the representative model of Dr. James Michels is introduced. Next, the physical model developed by Scientific Studies Corporation (SSC) [2] will be briefly discussed. We will refer to it in the remainder of this report as the physical model. Finally, a third technique, which makes use of both the physical model and the representative model, is introduced [3]. This approach will be referred to as the hybrid model. This set of data signal generation forms the basis of our simulation capability tool.

This data simulation tool is capable of generating time series data as viewed by a linear phased array on an airborne moving platform. To avoid ambiguities and for completeness of the work, the same notation as that developed by SSC will be used in this report. Using the representative model for example, the idea is to generate data directly from

a specified covariance matrix for evaluations of STAP algorithms. The method provides control of both spatial and temporal correlation as well as the probability density function (pdf) of the processes. Parameters such as partial temporal and spatial correlation of signal and interference resulting from the observation platform motion, beam pointing and internal clutter motion are also included.

This report is organized as follows. Chapter 2 describes the models for signal generation used in this effort. Examples involving the representative model will be introduced in section 3. True covariance computation and time series data generation are discussed in Chapter 4. In chapter 5, several techniques for data generation will be discussed. In chapter 6 we show some examples using the proposed models. Concluding remarks and recommendation for future work will be discussed in chapter 7.

# 2

# Phased Array Radar Model

In this section, a system model is developed. This system is commonly used for airborne surveillance pulsed-Doppler radars. The model is based on a side looking phased array radar configuration with a scanning capability of ±90°. Note that each component (target, jammer, clutter and noise) is modeled independently of the others. It is our goal and intent to generate true covariance matrices for each of these components as well as to generate a sequence of space-time independent data.

Targets are modeled as point targets in azimuth and elevation and for a wide range on scenarios. This includes the constant amplitude case and Swerling cases 1 through 4. Jamming signals are modeled as barrage type noise. This assumes point sources with Gaussian distributed wide-band noise in both azimuth and elevation. Receiver noise is assumed to be uncorrelated in both time and space. Ground clutter is modeled as a large number of statistically independent clutter patches with each patch consisting of a large number of individual re-radiators.

The array is assumed to be linear uniformly spaced with element spacing denoted by d. It consists of J identical elements (or identical beamformed sub-arrays). The platform is assumed to be moving at a velocity $v_p$ at an altitude $H_p$. The array geometry is shown in Figure 1.

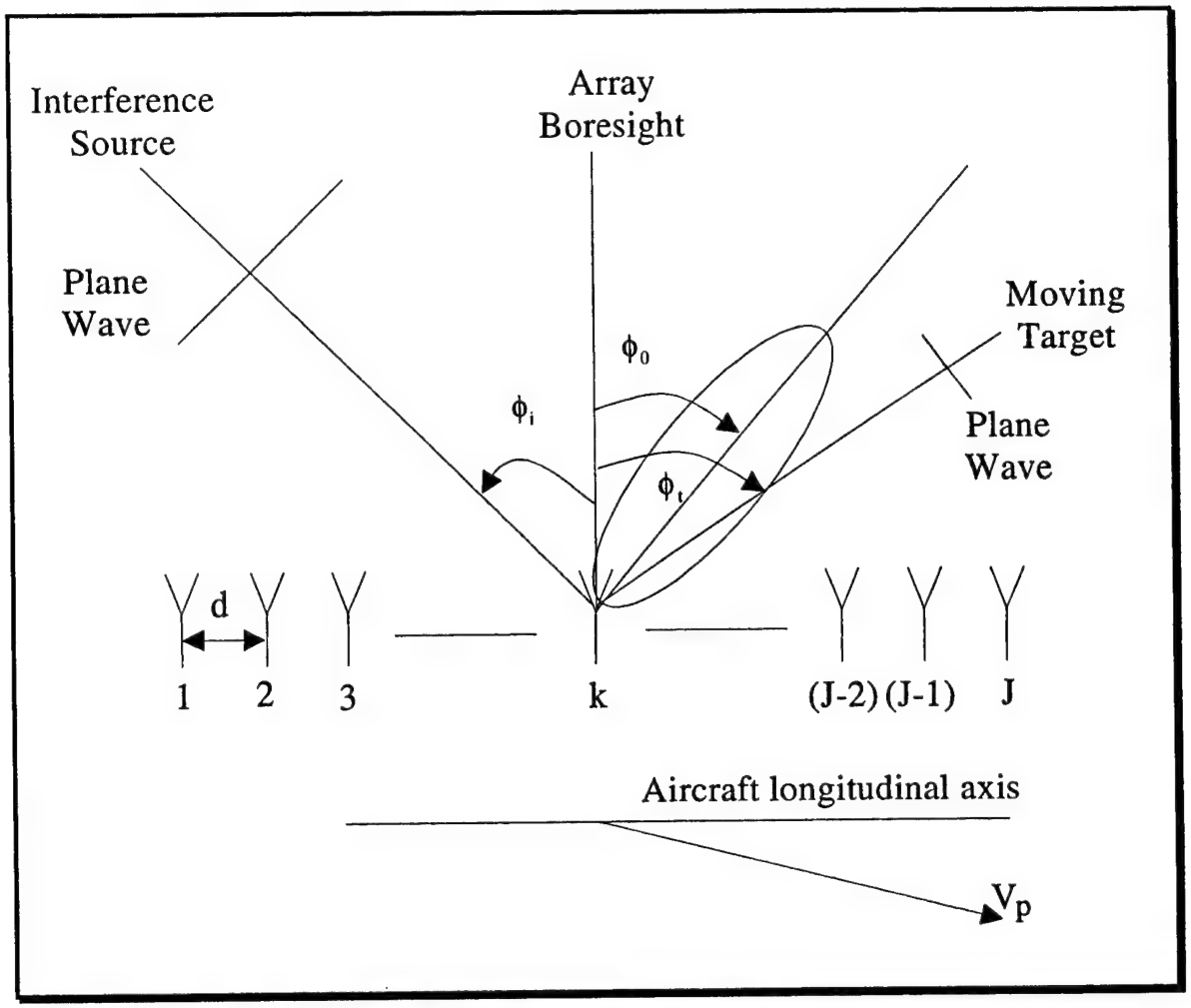


**Figure 1. Airborne Surveillance Scenario**

The antenna boresight is assumed to be normal to the platform direction. However, the platform velocity vector $v_p$ may have an offset angle from the platform direction. This results in a crab angle denoted by $\delta$.

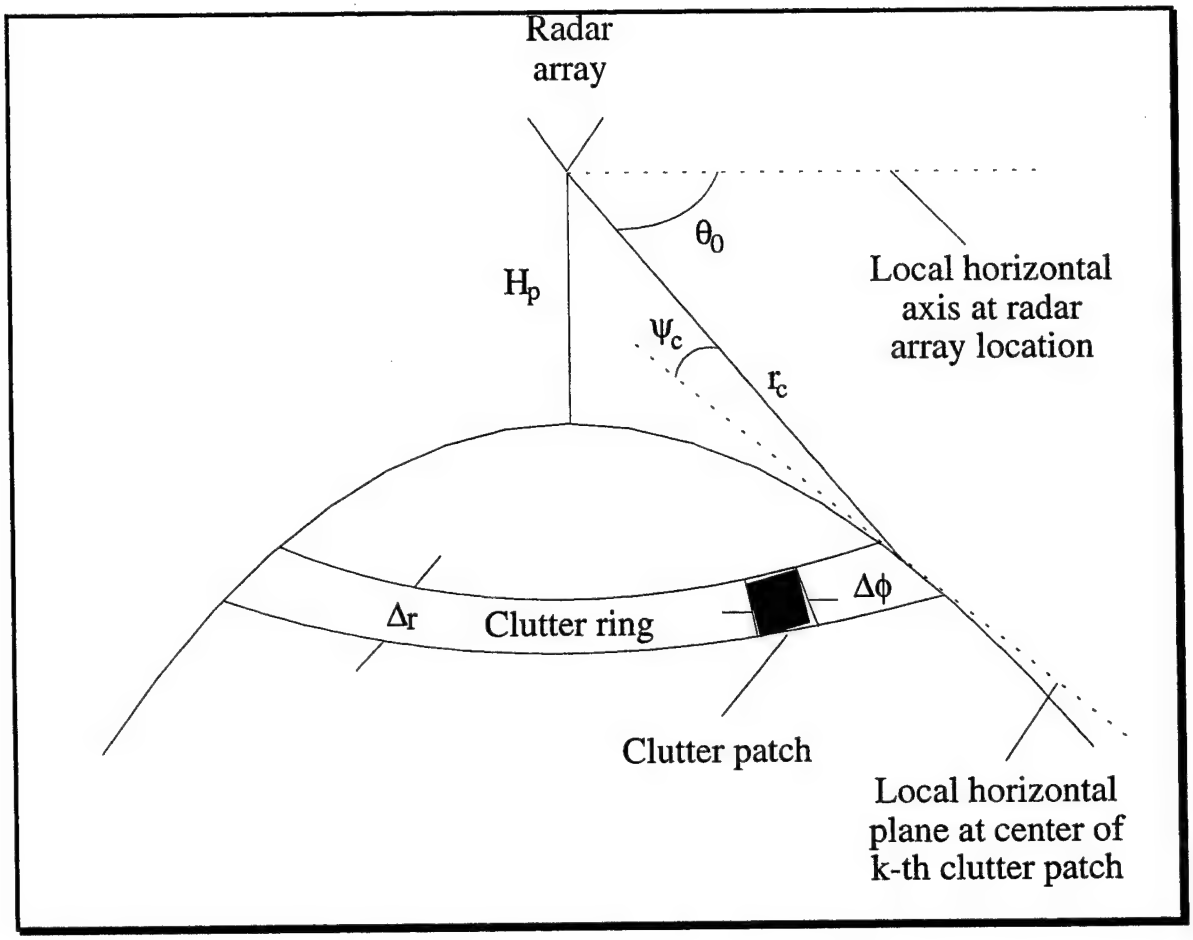


**Figure 2. Airborne surveillance geometry**

# 3

# Representative Model

The approach consists of first forming a two-dimensional (2-D) spatial and temporal correlation function with a corresponding 2-D spectrum as shown below.

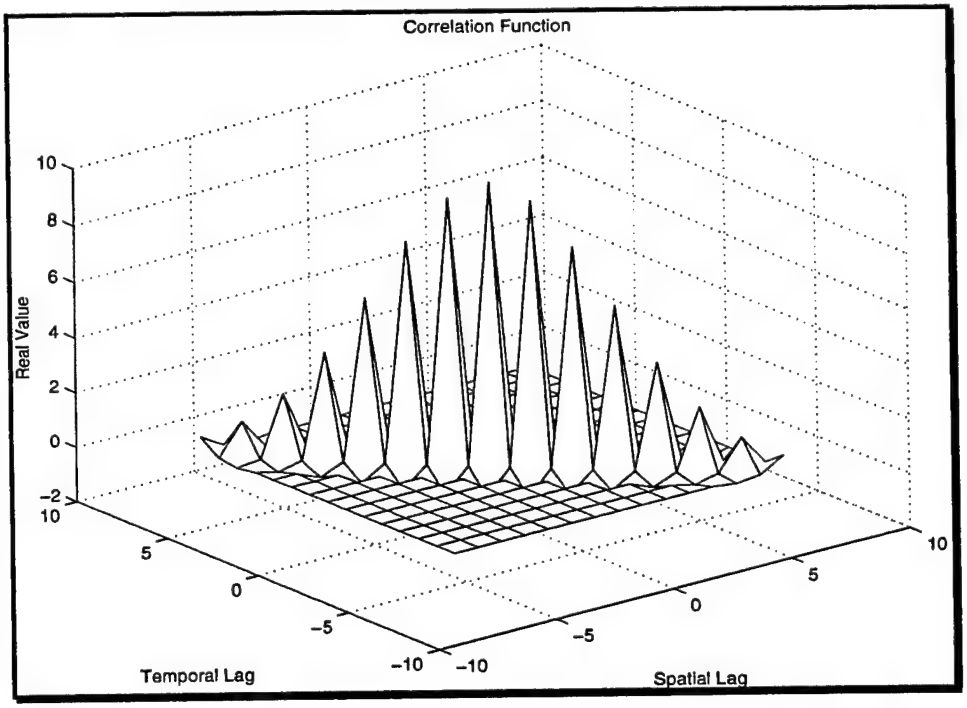


**Figure 3. Correlation function**

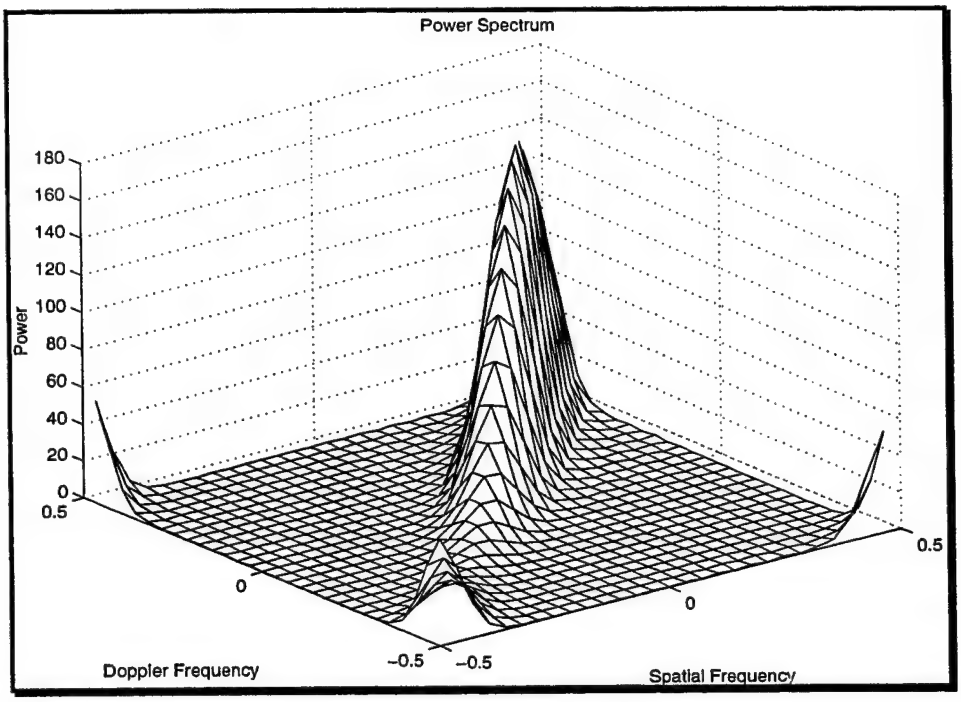


**Figure 4. Corresponding spectrum**

The term "*representative*" is used to denote the generic shaping of this correlation and its corresponding spectrum through the use of parametric functions referred to as "*shaping*" functions. This procedure, unlike the physical model, does not account for a detailed physical description that would then give rise to such a function. This approach shapes the correlation function with the intent to obtain profiles representative of those observed in practice. Figure 5 and 6 show the correlation function and its corresponding spectrum, respectively, for the case when the radar platform is stationary and the mainbeam is pointed at 0° (boresight).

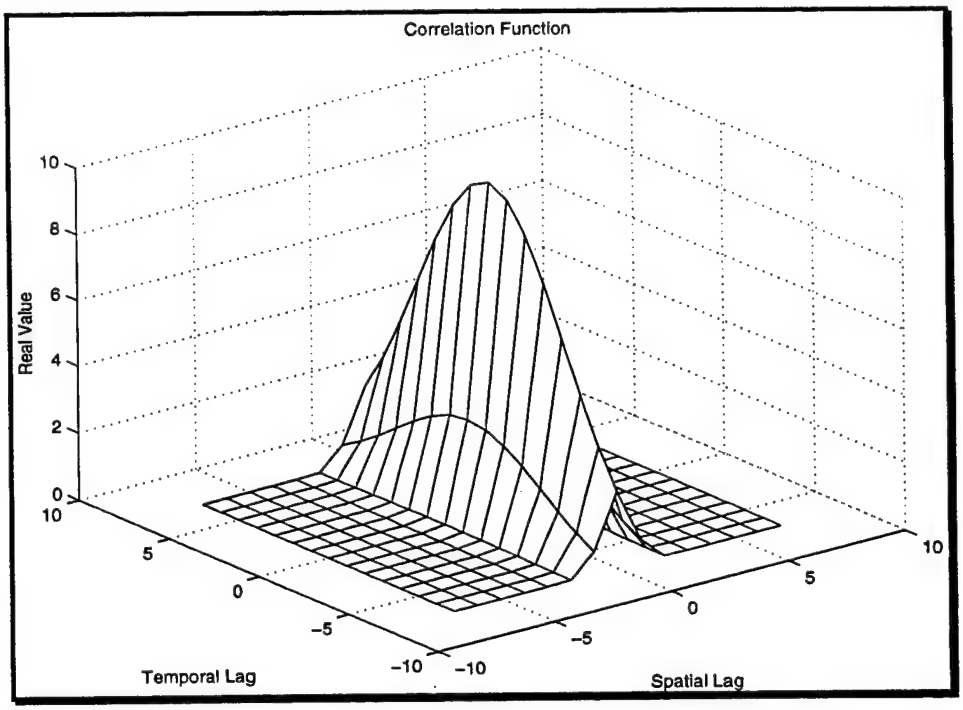


**Figure 5. Correlation function, stationary platform, $\phi = 0°$.**

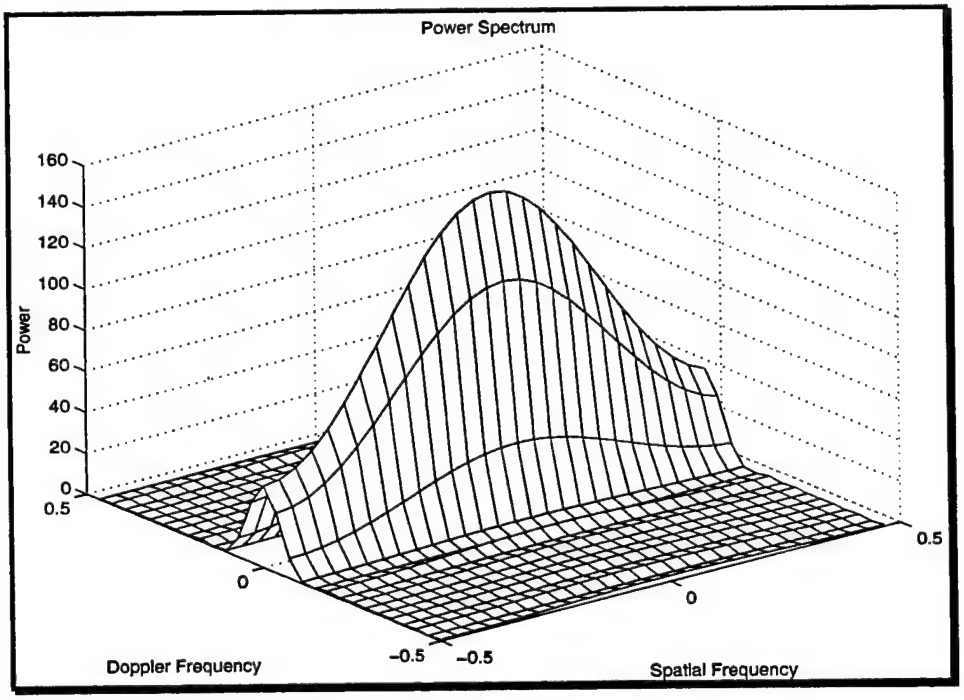


**Figure 6. Corresponding spectrum.**

Note from the above figures that the Doppler spread is due to internal clutter motion. The spatial distribution, on the other hand, is the result of the antenna beam profile.

To show the simplicity of the technique, assume that the platform is still stationary, but the mainbeam is pointed at and angle $\phi = 20°$. This results in the following spectrum in the angle-Doppler domain.

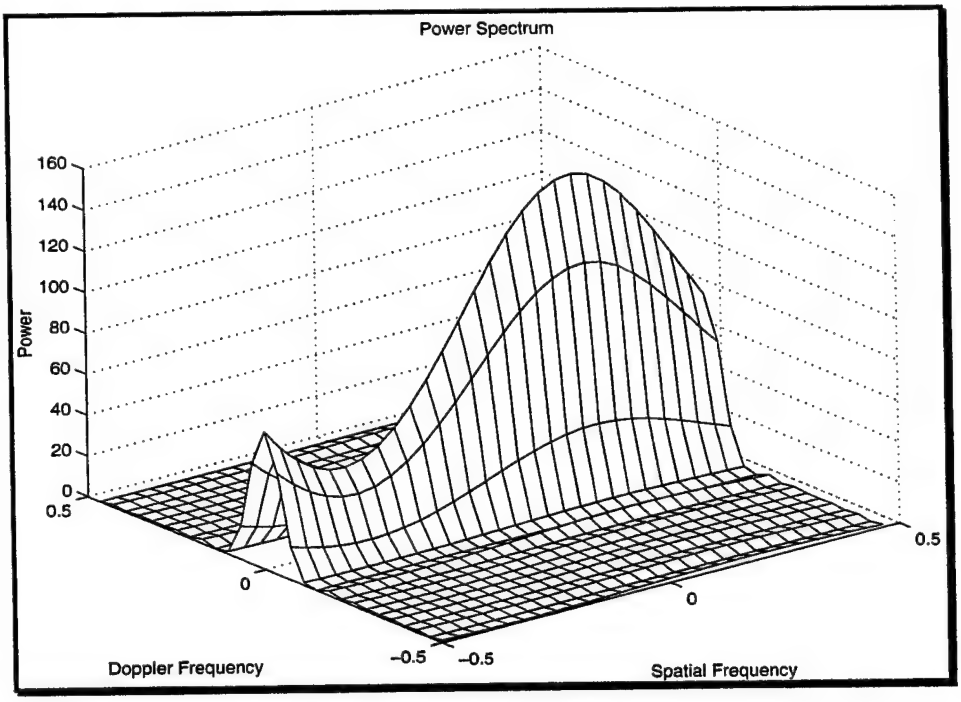


**Figure 7. Spectrum, $v_p = 0$, $\phi = 20°$.**

Assume now that the platform velocity is non-zero. This result in a Doppler-spatial frequency dependence that yields the rotated spectrum (see Figure 8 below).

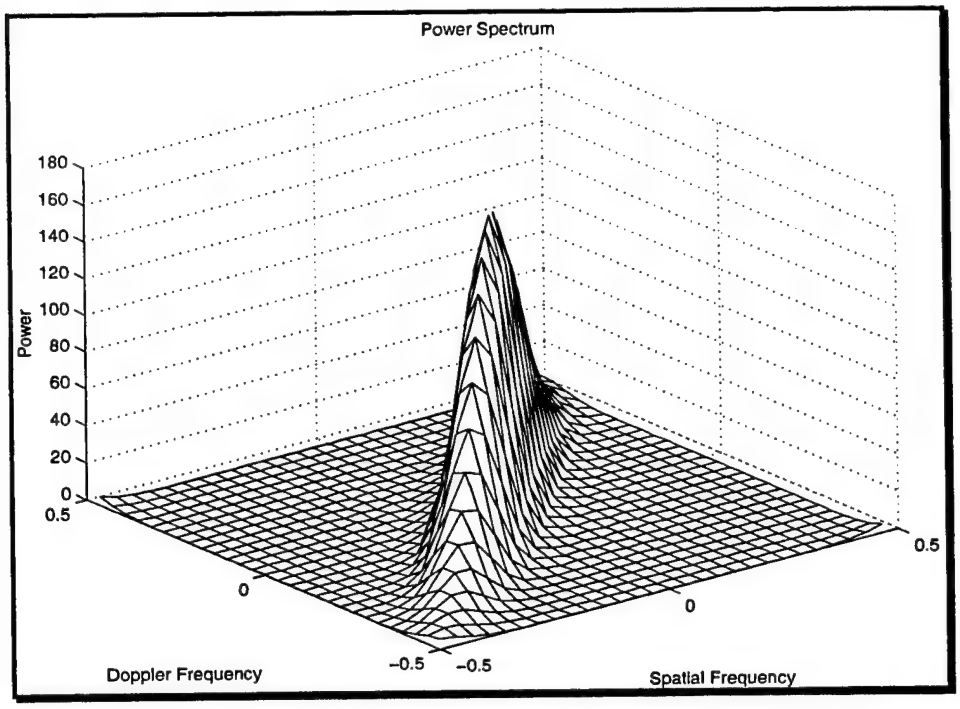


**Figure 8. Spectrum, $v_p \neq 0$, $\phi = 20°$.**

The shaping functions described above are used to control both the temporal and the spatial profiles of the correlation distributions. The values of the cross- and auto-correlation functions are then used as the elements of the multi-channel correlation matrix. This matrix is then used in the process synthesis procedures to generate time series data that contain the correlation specified in the matrix.

# 4

# Correlation Matrix Description

Define the zero-mean (Jx1) observation data vector $\underline{X}(n)$ at time n, under the null and alternative hypothesis $H_0$ and $H_1$, respectively, as

$$H_0: \quad \underline{X}(n)=\underline{C}(n)+\underline{I}(n)+\underline{W}(n) \quad ; \ n=1,2,\cdots,N \tag{1}$$

$$H_1: \quad \underline{X}(n)=\underline{S}(n)+\underline{C}(n)+\underline{I}(n)+\underline{W}(n) \ ; \ n=1,2,\cdots,N \tag{2}$$

where $\underline{S}(n)$ is the signal vector, $\underline{C}(n)$ is the temporally correlated clutter process, $\underline{I}(n)$ is the interference process and $\underline{W}(n)$ is the additive white noise process assumed to be uncorrelated in both space and time.

For a fully adaptive signal processor, a $(JNx1)$ concatenated observation data vector $\underline{X}$ is formed as

$$\underline{X}=\begin{bmatrix} \underline{X}(1) \\ \underline{X}(2) \\ \vdots \\ \underline{X}(N) \end{bmatrix}. \tag{3}$$

## 4.1 Signal Model

In this section, we review the different signal models employed in our simulations.

### 4.1.1 Constant Amplitude Signal

The signal model provides a (Jx1) vector time sequence $\underline{S}(n)$. For the constant amplitude signal model, we have

$$\underline{S}(n)=a\underline{U}(n) \tag{4}$$

where a represents the complex signal amplitude and the signal steering vector $\underline{U}(n)$ is given by

$$\underline{U}(n)=\underline{U}\exp\{j2\pi(n-1)\varpi_t\}. \tag{5}$$

Note from the above Equation that the spatial steering vector $\underline{U}$ is defined to be

$$U=\begin{bmatrix} 1 \\ \exp\{j2\pi\vartheta_t\} \\ \vdots \\ \exp\{j2\pi(J-1)\vartheta_t\} \end{bmatrix}. \quad (6)$$

In Equation (5) and (6), $\varpi_t$ and $\vartheta_t$ denote the normalized target Doppler and spatial frequencies as viewed from the platform, respectively, and are given by

$$\varpi_t = T\{f_t + f_p \cos(\theta_t)\sin(\phi_t - \gamma)\} \quad (7)$$

and

$$\vartheta_t = (d/\lambda)\cos(\theta_t)\sin(\phi_t - \gamma). \quad (8)$$

In the above Equations, the frequencies $f_t$ and $f_p$ are given by

$$f_t = (2v_t/\lambda_c) \quad (9)$$

and

$$f_p = (2v_p/\lambda_c). \quad (10)$$

The complex signal amplitude a can be expressed as

$$a = A\exp(j\delta_0) \quad (11)$$

where A is the magnitude and $\delta_0$ is the initial phase. Therefore the k-th channel signal is expressed as

$$s_k(n) = A\exp(j\delta_0)\exp\{j2\pi(k-1)\vartheta_t\}\exp\{j2\pi(n-1)\varpi_t\};\ n=1,2,\cdots,N,\ k=1,2,\cdots,J. \quad (12)$$

4.1.2

## Case 1: Constant Amplitude, Random Phase Signal Model

In the constant amplitude, random phase signal model, A is kept constant over both the time pulses of the CPU as well as over multiple ensemble realizations (i.e., over multiple CPI's). The phase $\delta_0$ is kept constant over the time pulses of the CPI, but is assumed to be a random variable uniformly distributed in the interval $(0, 2\pi)$, over multiple ensemble realizations.

4.1.3

### Case 2: Constant Amplitude, Constant Phase Signal Model

In the constant amplitude, constant phase, signal model, both A and $\delta_0$ are kept constant over both the time pulses of the CPU as well as over multiple ensemble realizations (i.e., over multiple CPI's.

4.1.4

### Case 3: Swerling I Model

The Swerling I model characterizes a signal with perfect correlation pulse-to-pulse over a coherent processing interval (CPI) consisting of N pulses, but random over successive realizations. In this case, the amplitude A is modeled as a Rayleigh distributed random variable across realizations but kept constant over a given CPI. Its mean value is A. The phase $\delta_0$ is also kept constant over a single realization of N time samples (one CPI), but is a random variable uniformly distributed between $(0, 2\pi)$, over multiple ensemble realizations.

4.1.5

### Case 4: Swerling II Model

The Swerling II model characterizes a signal that is totally uncorrelated from pulse to pulse over a coherent processing interval (CPI) consisting of N pulses. In addition, it is also assumed to be a random variable over successive realizations. The amplitude A is modeled as a Rayleigh distributed random variable across realizations but kept constant over a given CPI. Its mean value is A. The phase $\delta_0$ is also assumed to be a random variable uniformly distributed between $(0, 2\pi)$, over multiple ensemble realizations.

5.1.6

### Case 5: Random Signal Model, Partial Temporal Correlation

The random signal model contains temporal correlation over the N time samples and is uncorrelated over multiple realizations.

## 4.2 Interference Model

The partially correlated noise jamming signal model is defined as

$$\tilde{I}_m(n,\theta_i) = I(n) \bullet \exp\{j2\pi(m-1)\vartheta_i\} \bullet \exp[j\pi(n-1)\varpi_i] \qquad (13)$$

where $I(n)$ is a complex noise process with partial temporal correlation, $\vartheta_i$ is the normalized interference source spatial frequency and $\varpi_i$ is the normalized interference center Doppler frequency. The quantities $\vartheta_i$ and $\varpi_i$ can be expressed as

$$\vartheta_i = (d/\lambda)\cos(\theta_i)\sin(\phi_i) \tag{14}$$

and

$$\varpi_i = (v_i/\lambda)T + (2v_p/\lambda)T\cos(\theta_i)\sin(\phi_i), \tag{15}$$

where $v_p$ is the platform velocity and $v_i$ is the interference source velocity. For white noise barrage jamming signals, we have

$$\tilde{I}_m(n,\theta_i) = I(n) \bullet \exp\{j2\pi(m-1)\vartheta_i\} \tag{16}$$

where $I(n)$ is a complex white noise process.

## 4.3 Clutter Model

In the following, three (3) procedures for the determination of the known clutter covariance matrix applicable for the airborne radar problem are described. Specifically, the auto- and cross-correlation functions for the clutter, signal and interference sources as viewed from airborne phased array radars are developed. These functions will then be used to form the known covariance matrices for data synthesis. These include (1) the representative model, (2) the physical model and (3) the hybrid model. These methods lead to a procedure for the generation of a clutter time series with correlation provided by the known covariance matrix. Note that Dr. James Michels has suggested both the representative model and the hybrid model. Scientific Studies Corporation Inc. (SSC) has coded the physical model. Minor changes have been made to this code to fit both the Rome Laboratory Space-Time Adaptive Processing (RLSTAP) needs and our own needs.

In this section, the expressions for the auto- and cross-correlation functions between side mounted airborne sub-arrays are derived. Note that only azimuth variations within a given range resolution cell are considered. Two approaches are discussed. The first approach does not take into account the effect of platform crab angle and the second considers this effect. First, we do not consider the effects of platform crab angle.

Let $\tilde{c}_k(n)$ denote the complex baseband clutter process from the k-th channel at time n. Assuming stationarity, the clutter cross- channel correlation function between channels k and i is given by

$$R_{c,ki}(l_t)=E\{\tilde{c}_k(n)\tilde{c}_i^*(n-l_t)\}=E\{\tilde{c}_k(n+l_t)\tilde{c}_i^*(n)\},$$

where $l_t$ is the temporal lag value. A functional form for the correlation function $R_{c,ki}(l_t)$ is now proposed. To this end, let $\phi_0$ be the azimuth angle to the center of the beam position as measured from boresight of the antenna. The cross-correlation function between the k-th and i-th channels is expressed as

$$R_{c.ki}(l_t)=\sigma_{c,k}\sigma_{c,i}F_c(l_t,k,i)\exp\left\{j2\pi(k-i)\frac{d}{\lambda}\sin(\phi_0)\right\}\exp\left\{j2\pi l_t T\frac{2v_p}{\lambda}\sin(\phi_0)\right\} \qquad (17)$$
$$(-N+1)\le l_t\le(N-1)$$

where

- $\sigma_{c,k}$ and $\sigma_{c,i}$ are the standard deviations of the clutter process as observed on channels k and i, respectively
- $l_t$ is the temporal lag
- $F_c(l_t,l_s)$ is a two-dimensional function of $l_t$ and $l_s$ for the clutter which shapes the magnitude of the clutter cross-correlation function in both the temporal and spatial domain, also referred to as the shaping function
- T is the inter-pulse period
- $v_p$ is the platform velocity
- $\lambda=(c/f_0)$ is the transmitter wavelength, $f_0$ is the transmitter frequency and c is the speed of light
- d is the inter-element spacing
- $\phi_0$ is the center of the beam position in azimuth.

Let $l_s$ be the spatial lag, i.e.; $l_s=(k-i)$, then Equation (17) becomes

$$R_c(l_t,l_s)=\sigma_{c,k}\sigma_{c,i}F_c(l_t,l_s)\exp\left\{j2\pi l_s\frac{d}{\lambda}\sin(\phi_0)\right\}\exp\left\{j2\pi l_t T\frac{2v_p}{\lambda}\sin(\phi_0)\right\} \qquad (18)$$
$$(-N+1)\le l_t\le(N-1)\ ;\ (-M+1)\le l_s\le(M-1)$$

The two-dimensional (2-D) power spectral density $S(f_t, f_s)$ is obtained by taking the 2-D FFT of $R_c(l_t, l_s)$. The frequencies $f_t$ and $f_s$ are referred to as the temporal (Doppler) and spatial frequencies and are given by

$$f_t = \frac{2v_p}{\lambda}\sin(\phi_0) \tag{19}$$

and

$$f_s = \frac{d}{\lambda}\sin(\phi_0), \tag{20}$$

respectively.

Using Equations (19) and (20), it can be easily shown that

$$f_t = \left[T\frac{2v_p}{d}\right]f_s. \tag{21}$$

Let $\tan(\alpha)$ be the quantity

$$\tan(\alpha) = \left[T\frac{2v_p}{d}\right]. \tag{22}$$

Then $f_t$ and $f_s$ are related through the equation $f_t = \tan(\alpha)f_s$. Note that $\tan(\alpha)$ is the slope of the clutter in the normalized Doppler-spatial frequency domain.
Therefore $\alpha$ is given by

$$\alpha = \tan^{-1}\left(T\frac{2v_p}{d}\right). \tag{23}$$

For a non-zero platform crab angle, $\psi_c$, $\sin(\phi_0)$ in the above equations is replaced by $\sin(\phi_0 + \psi_c)$. This results in a non-linear relation between $f_t$ and $f_s$ in Equation (23). This results in a power spectrum that is no longer centered along the linear slope in the normalized Doppler-spatial frequency domain, but rather, along the arced curve. This case will discussed further in the next section.

Next, we introduce the coordinates $(l_A, l_B)$, in which the correlation function remains separable in time and space. The 2-D shaping function is expressed as

$$F_c(l_A, l_B) = F_{c,t}(l_A)F_{c,s}(l_B), \tag{24}$$

where the corresponding rotation in the correlation space is achieved using

$$\begin{bmatrix} l_A \\ l_B \end{bmatrix} = \begin{bmatrix} \cos(\alpha) & -\sin(\alpha) \\ \sin(\alpha) & \cos(\alpha) \end{bmatrix} \begin{bmatrix} l_t \\ l_s \end{bmatrix}. \tag{25}$$

Then, Equation (18) is rewritten as

$$F_c(l_t, l_s) = F_{c,t}\{l_t \cos(\alpha) - l_s \sin(\alpha)\} F_{c,s}\{l_t \sin(\alpha) + l_s \cos(\alpha)\}. \tag{26}$$

If the platform is not moving, $v_p = 0$, therefore $\alpha = 0$, Equation (26) becomes

$$F_c(l_t, l_s) = F_{c,t}(l_t) F_{c,s}(l_s). \tag{27}$$

This shows that $F_c(l_t, l_s)$ is separable.

### 4.3.1 Temporal Shaping Functions

Temporal shaping functions can take on several distributions. For a Gaussian shaped clutter power spectrum, the temporal function $F_{c,t}(\bullet)$ is also Gaussian. In this case, $F_{c,t}(l_A)$ can then be expressed as

$$F_{c,t}(l_A) = (\mu_{c,t})^{(l_A - l_{A,mi})^2}. \tag{28}$$

The parameter $\mu_{c,t}$ is the one-lag temporal correlation clutter parameter that controls the width of the correlation function magnitude along the $l_A$ axis and has range $0 \le \mu_{c,t} \le 1$. The parameter $l_{A,mi}$ is the temporal lag at which the magnitude of the clutter cross-correlation function achieves its peak value. For the phased array radar problem considered here, the parameter $l_{A,mi}$ is negligible. It is important for cases where receiver elements are widely spaced. In this case the time delay between channels is considerable. Only the case of $l_{A,mi} = 0$ is considered in this section.

In the case of a Gaussian shaped function, the parameter $\mu_{c,t}$ is expressed as

$$\mu_{c,t} = \exp\{-2\pi\xi^2 T^2\}, \tag{29}$$

where $\xi^2$ is the variance of the Gaussian shaped power spectrum measured along the temporal frequency axis $f_t$. Note that the form of Equation (18) will change for other shaping functions. In the case of an exponentially shaped function, $F_{c,t}(\bullet)$ is expressed as

$$F_{c,t}(l_A) = (\mu_{c,t})^{|l_A|} \tag{30}$$

where

$$\mu_{c,t} = \exp\{-2\pi\xi T\}. \tag{31}$$

Therefore, $F_{c,t}(l_A)$ is given by

$$F_{c,t}(l_A) = \frac{\alpha^2}{\alpha^2 + (2\pi l_A)^2}. \tag{32}$$

### 4.3.2 Spatial Shaping Functions

The spatial shaping functions for the clutter $F_{c,s}(l_s)$ is expressed as

$$F_{c,s}(l_s) = |G_T(l_s)|^2 |G_k(\phi_0) G_i^*(\phi_0)|, \tag{33}$$

which can also be written as

$$F_c^s(l_s) = |G_T(l_s)|^2 \cos^2(\phi_0). \tag{34}$$

In Equations (33) and (34), the term $|G_T(l_s)|^2$ is the transmitter magnitude gain term in the correlation domain whereas the complex receive gain terms $G_k(\phi_0)$ and $G_i(\phi_0)$ for channels k and i, respectively, are assumed to have uniform unit amplitude gain on each channel. The term $\cos(\phi_0)$ represents the individual element receiver gain for a dipole pattern. The term $|G_T(l_s)|^2$ can be expressed as

$$|G_T(l_s)|^2 = \left\{\beta + (1-\beta)\cos\left[\pi \frac{l_s}{M-1}\right]\right\}^2 \quad ; \quad (-M+1) \le l_s \le (M-1). \tag{35}$$

Note in the above Equation that it is possible to implement the Hanning $(\beta = 0.5)$, Hamming $(\beta = 0.543478261)$ and Blackman-Harris $(\beta = 0.53856)$ element weighted gain profiles.

In the $(l_A, l_B)$ coordinate system, we have

$$|G_T(l_B)|^2 = \left\{\beta + (1-\beta)\cos\left[\pi \frac{l_B}{(N-1)\sin(\alpha) + (M-1)\cos(\alpha)}\right]\right\}^2 \tag{36}$$

for

$$-[(N-1)\sin(\alpha) + (M-1)\cos(\alpha)] \le l_B \le [(N-1)\sin(\alpha) + (M-1)\cos(\alpha)].$$

For a Gaussian shaped spatial function, we have

$$F_{c,s}(l_B)=(\mu_{c,s})^{(l_B)^2}\cos^2(\phi_0)$$

where $(\mu_{c,s})$ is defined as the one-lag correlation clutter parameter and has range $(0\le\mu_{c,s}\le 1)$. The parameter $(\mu_{c,s})$ has the same role as $(\mu_{c,t})$. Whereas $(\mu_{c,t})$ controls the width of the temporal frequency spectrum, $(\mu_{c,s})$ controls the width of the spatial frequency spectrum related to the beam width.

### 4.3.3 Correlation Functions

The cross-correlation function between channels k and i is given by

$$R_{c,ki}(l_t,l_s)=\sigma_{c,k}\sigma_{c,i}F_{c,t}\{l_t\cos(\alpha)-l_s\sin(\alpha)\}F_{c,s}\{l_t\sin(\alpha)+l_s\cos(\alpha)\}$$
$$\bullet\exp\left\{j2\pi l_s\frac{d}{\lambda}\sin(\phi_0)\right\}\exp\left\{j2\pi l_t T\frac{2v_p}{\lambda}\sin(\phi_0)\right\} \qquad (37)$$

The first complex exponential contains the phase delay between the elements from a source with phase coming from $\phi=\phi_0$. This results in a peak in the spatial spectrum at

$$f_s=T\frac{d}{\lambda}\sin(\phi_0). \qquad (38)$$

The second complex exponential term contains the pulse to pulse phase delay due to the platform velocity. This again results in a peak at $f_t=f_{dc}$, where $f_{dc}$ is given by

$$f_{dc}=T\frac{2v_p}{\lambda}\sin(\phi_0). \qquad (39)$$

Note that $f_{dc}$ is the center of the Doppler shifted clutter spectrum.

The terms $\sigma_{c,k}$ and $\sigma_{c,i}$ control the magnitude of the cross-correlation function that itself controlled by the temporal and spatial functions $F_t(\bullet)$ and $F_s(\bullet)$, respectively. As was mentioned before, the width of the spectrum, along the temporal frequency $f_t$, is due to the internal motion of the clutter, described by $F_t(\bullet)$, and the platform motion induced Doppler spread from all azimuth angles viewed by the antenna beam pattern and is described by $F_s(\bullet)$. The latter is the dominant contributor to the width of the spectrum in the angle/Doppler domain. Note that a narrow width in the correlation domain corresponds to a wide spectral width. Since the width in the correlation function $R_c(l_t,l_s)$ along the $l_t$ and $l_s$

axes, is determined by the product $F_t(\bullet)\,F_s(\bullet)$, the narrowest of these two functions in the correlation domain yields the large spectral width.

Consider now the auto-correlation function; i.e., k = i. In this case, Equation (37) becomes

$$R_{c,kk}(l_t,l_s)=\sigma_{c,k}^2 F_{c,t}\{l_t\cos(\alpha)-l_s\sin(\alpha)\}F_{c,s}\{l_t\sin(\alpha)+l_s\cos(\alpha)\} \bullet\exp\left\{j2\pi l_s\frac{d}{\lambda}\sin(\phi_0)\right\}\exp\left\{j2\pi l_t T\frac{2v_p}{\lambda}\sin(\phi_0)\right\} \quad (40)$$

To further simplify this equation, let $l_s=k-i=0$. In this case,

$$\exp\left\{j2\pi l_s\frac{d}{\lambda}\sin(\phi_0)\right\}=1, \quad (41)$$

and Equation (40) becomes

$$R_{c,kk}(l_t)=\sigma_{c,k}^2 F_{c,t}\{l_t\cos(\alpha)\}F_{c,s}\{l_t\sin(\alpha)\}\exp\left\{j2\pi l_t T\frac{2v_p}{\lambda}\sin(\phi_0)\right\}. \quad (42)$$

Note from Equation (42) that the auto-correlation function has no dependence on $l_s$. Assume now that $v_p=0$, this implies that $\alpha=0$. The function $F_{c,s}\{l_t\sin(\alpha)\}$ is unity and the function $F_{c,t}\{l_t\cos(\alpha)\}$ reduces to $F_{c,t}(l_t)$. In this case, the width of the auto-correlation function is only dependent on the internal clutter motion. For the case where $l_t=0$, Equation (42) reduces to

$$R_{c,kk}(l_t)=R_{c,k}(l_t)=\sigma_{c,k}^2, \quad (43)$$

which is the variance of the clutter process. Equations (42) and (43) provide analytic expressions for the elements of the clutter covariance matrix for the k-th range $R_{c,k}$. In section 5, this matrix will be used to develop several procedures for data synthesis.

### 4.3.4 Physical Model Clutter Covariance Matrix

In this section, a brief description of the SSC physical model will be given. For a complete description of the technique, please see []. The equations that will be described here are provided here for convenience only.

Let the JxJ clutter covariance matrix be given by

$$R_c(m)=E\left[\underline{c}(n)\underline{c}^H(n-m)\right]=\sum_{p=0}^{N_c-1}\sigma_{cp}^2\exp\left\{j2\pi m\varpi_p\right\}\underline{e}_J(\vartheta_p)\underline{e}_J^H(\vartheta_p) \tag{44}$$

where

$$\underline{e}_J(\vartheta_p)=\begin{bmatrix}1\\ \exp\{j2\pi\vartheta_p\}\\ \vdots\\ \exp\{j2\pi(J-1)\vartheta_p\}\end{bmatrix}. \tag{45}$$

In the above Equations, the following quantities are defined as

$$\varpi_p=\frac{1}{2}\upsilon\cos(\theta_0)\sin(\phi_p-\gamma)\quad ;\quad p=0,1,\cdots,(N_c-1) \tag{46}$$

$$\vartheta_p=\frac{d}{\lambda_c}\cos(\theta_0)\sin(\phi_p)\quad ;\quad p=0,1,\cdots,(N_c-1) \tag{47}$$

$$\phi_p=-\pi+p\Delta\phi \tag{48}$$

$$\theta_0=-\sin^{-1}\left\{\frac{r_c^2+H_p(H_p+2r_E)}{2r_c(H_p+r_E)}\right\} \tag{49}$$

$$\Delta\phi=\frac{\pi}{(N_c-1)} \tag{50}$$

$$\upsilon=\frac{4v_p}{\lambda_c f_{PRF}}. \tag{51}$$

The power of the p-th clutter return and the clutter to noise ratio (CNR) are defined as

$$\sigma_{cp}=\sigma_n^2\xi_c(\phi_p,\theta_0) \tag{52}$$

and

$$\xi_c(\phi_p,\theta_0)=\frac{P_tT_u\lambda_c^2\zeta_cG_t(\phi_p,\theta_0)g_r(\phi_p,\theta_0)}{(4\pi)^2N_0L_sr_c^4}, \tag{53}$$

respectively.

$$\zeta_c=s_0W_cL_c \tag{54}$$

$$s_0=\gamma_c\sin(\psi) \tag{55}$$

$$\psi=\sin^{-1}\left\{\frac{H_p}{r_c}\left(1+\frac{H_p}{2r_E}\right)-\frac{r_c}{2r_E}\right\} \tag{56}$$

$$W_c = \frac{2\pi r_c}{N_c} \tag{57}$$

$$L_c = \begin{cases} \dfrac{\rho_r}{\cos(\psi_c)} = \dfrac{v}{2f_B \cos(\psi_c)} & \text{if} \quad \rho_r \tan(\psi_c) \le r_c \tan(\beta_{1e}) \\ \dfrac{2r_c \tan(\beta_{1e}/2)}{\sin(\psi_c)} & \text{if} \quad \rho_r \tan(\psi_c) > r_c \tan(\beta_{1e}) \end{cases} . \tag{58}$$

$$\rho_r = \frac{v}{2f_b} \tag{59}$$

$$G_t(\phi_p, \theta_0) = G_0 G_a(\phi_p, \theta_0) g_e(\phi_p, \theta_0). \tag{60}$$

For uniform array pattern, $G_a(\phi_p, \theta_0)$ is given by

$$G_a(\phi_p, \theta_0) = \begin{cases} \left| \dfrac{\sin\left\{\dfrac{J\pi d}{\lambda_c}\left[\sin(\phi_p) - \sin(\phi_0)\right]\right\}}{J \sin\left\{\dfrac{\pi d}{\lambda_c}\left[\sin(\phi_p) - \sin(\phi_0)\right]\right\}} \right|^2 & \text{for} \quad -90° \le \phi_p \le 90° \\ G_b \left| \dfrac{\sin\left\{\dfrac{J\pi d}{\lambda_c}\left[\sin(\phi_p) - \sin(\phi_0)\right]\right\}}{J \sin\left\{\dfrac{\pi d}{\lambda_c}\left[\sin(\phi_p) - \sin(\phi_0)\right]\right\}} \right|^2 & \text{for} \quad 90° \le \phi_p \le 270° \end{cases} . \tag{61}$$

For a Dolph-Chebychev array pattern, $G_a(\phi_p, \theta_0)$ is given by

$$G_a(\phi_p, \theta_0) = \begin{cases} \dfrac{1}{U} \left| F\left[\underline{e}_J(f_{s0}) \otimes \underline{u}\right] \right|^2 & \text{for} \quad -90° \le \phi_p \le 90° \\ G_b \dfrac{1}{U} \left| F\left[\underline{e}_J(f_{s0}) \otimes \underline{u}\right] \right|^2 & \text{for} \quad 90° \le \phi_p \le 270° \end{cases} , \tag{62}$$

where

F is the discrete Fourier transform (DFT) operator, $\otimes$ is the Shur (element by element) product, and $\underline{u}$ is the J-dimensional vector of Dolph-Chebychev weights.

$$\underline{e}_J(f_{s0}) = \begin{bmatrix} 1 \\ \exp\{j2\pi f_{s0}\} \\ \vdots \\ \exp\{j2\pi(J-1)f_{s0}\} \end{bmatrix} \tag{63}$$

with

$$f_{s0} = (d/\lambda)\cos(\phi_0)\sin(\phi_0) \tag{64}$$

$g_e(\phi_p, \theta_0)$ is the element power pattern given by

$$g_e(\phi_p, \theta_0) = \begin{cases} \cos^2(\phi_p) & \text{for } -90° \le \phi_p \le 90° \\ G_b \cos^2(\phi_p) & \text{for } 90° \le \phi_p \le 270° \end{cases}. \tag{65}$$

$g_r(\phi_p, \theta_0) = g_e(\phi_p, \theta_0)$ is the receive element power pattern.

### 4.3.5 Hybrid Clutter Model

In this section, the hybrid clutter model is described. This model is referred to as the hybrid due to the fact that it combines the inherent simplicity of the representative model with the sophistication of the physical model. To this end, let the (JxJ) clutter covariance matrix $R_c(m) = E\{\underline{c}(n)\underline{c}^H(n-m)\}$ be given by

$$R_c(m) = \sigma_c^2 \frac{\sum_{p=0}^{N_c-1} F_t(m, \phi_p, \theta_0) F_s(\phi_p) \exp\{j2\pi m \varpi_p\} \underline{e}_J(\vartheta_p) \underline{e}_J^H(\vartheta_p)}{\sum_{p=0}^{N_c-1} F_s(\phi_p)} \quad ; \quad m > 0 \tag{66}$$

where m is the temporal lag and the vector $\underline{e}_J(\vartheta_p)$ is defined as

$$\underline{e}_J(\vartheta_p) = \begin{bmatrix} 1 \\ \exp\{j2\pi\vartheta_p\} \\ \vdots \\ \exp\{j2\pi(J-1)\vartheta_p\} \end{bmatrix}. \tag{67}$$

# 5

# Estimation Methods

In this section, we describe the estimation methods used. To achieve this, we first show how we utilize the analytic expressions developed earlier in a process synthesis procedure. This will involve generation of both clutter and partially correlated signal and interference data as observed from a phased array radar. Let $x_{k,m}(n)$ be a zero-mean Gaussian complex-valued sample representing clutter, target, or an interference signal observed from the m-th channel corresponding to the k-th range cell at time n. Consider the space-time data vector at range cell k.

$$\underline{X}_k = \begin{bmatrix} \underline{x}_k(1) \\ \underline{x}_k(2) \\ \vdots \\ \underline{x}_k(N) \end{bmatrix} \tag{68}$$

where each entry $\underline{x}_k(n)$ is a Jx1 spatial vector given by

$$\underline{x}_k(n) = \begin{bmatrix} x_{k,1}(n) \\ x_{k,2}(n) \\ \vdots \\ x_{k,J}(n) \end{bmatrix} \tag{69}$$

and J and N are the number of channels and pulses, respectively.

Consider now the JNxJN Hermitian block Toeplitz correlation matrix

$$R_k = E\left[\underline{X}_k \underline{X}_k^H\right] = \begin{bmatrix} R_k(0) & R_k(-1) & \cdots & R_k(-N+1) \\ R_k(1) & R_k(0) & \cdots & R_k(-N+2) \\ \vdots & \vdots & \cdots & \vdots \\ R_k(N) & R_k(N-1) & \cdots & R_k(0) \end{bmatrix} \tag{70}$$

where each JxJ block of $R_k$ can be expressed as

$$R_k(n) = \begin{bmatrix} R_{11}(n) & R_{12}(n) & \cdots & R_{1J}(n) \\ R_{21}(n) & R_{22}(n) & \cdots & R_{2J}(n) \\ \vdots & \vdots & \cdots & \vdots \\ R_{J1}(n) & R_{J2}(n) & \cdots & R_{JJ}(n) \end{bmatrix}; \; n = 0,1,\ldots,(N-1). \tag{71}$$

Next, we discuss two methods for data generation.

## 5.1 Block Procedure for Clutter Generation

The block procedure for generating clutter and partially target or interference processes is very useful in generating independent identically distributed (iid) radar data. It is also one of the fastest data generation technique for quick check up and analysis. Given a known clutter covariance matrix, the objective is to factorize this matrix using techniques such as Cholesky decomposition, an LDL decomposition, an eigen-decomposition or a singular value (SVD) decomposition. Whereas some techniques have more merit than others do, we have shown through our computer simulations that the SVBD is the most robust. This in turn leads to more stable results. Once the factorization is complete, driving a white noise process through this system generates radar data. The specific steps involved in this technique are described below:

1. Given the elements of the JNxJN clutter correlation matrix at range k, $R_K^c$, we form the SVD of $R_K^c$,

$$R_k^c = USU^H = \left(US^{1/2}\right)\left(US^{1/2}\right)^H. \tag{72}$$

2. Generate a data vector $\underline{X}_k$ as

$$\underline{X}_k = \left(US^{1/2}\right)\underline{W}_k, \tag{73}$$

where $\underline{W}_k$ is a JNx1 Gaussian white noise vector with zero-mean and unit variance. In vector form, Equation (49) can be written as

$$\underline{X}_k = \begin{bmatrix} \underline{x}_k(1) \\ \underline{x}_k(2) \\ \vdots \\ \underline{x}_k(N) \end{bmatrix} = \left(US^{1/2}\right)\underline{W}_k = \left(US^{1/2}\right)\begin{bmatrix} \underline{w}_k(1) \\ \underline{w}_k(2) \\ \vdots \\ \underline{w}_k(N) \end{bmatrix}, \tag{74}$$

where

$$\underline{x}_k(n) = \begin{bmatrix} x_{k1}(n) \\ x_{k2}(n) \\ \vdots \\ x_{kJ}(n) \end{bmatrix}$$

and

$$\underline{w}_k(n) = \begin{bmatrix} w_{k1}(n) \\ w_{k2}(n) \\ \vdots \\ w_{kJ}(n) \end{bmatrix}.$$

The elements of the concatenated JNx1 vector $\underline{X}_k$ consists of the processes containing the correlation specified by the clutter correlation matrix $R_K^c$.

## 5.2 Time Series Procedure for Clutter Generation

Using this technique, the clutter signal returns are generated as multi-channel auto-regressive (AR) processes []. In what follows, we give a brief description of the proposed procedure.

1. The order P of the AR process is selected based upon a specified tolerance for fitting the desired spectrum.
2. The elements of a JNxJN matrix $R_k^P$ (this matrix is a subset of the matrix $R_k$) are specified using the analytic expressions developed in the previous sections.
3. Using the block Toeplitz form of $R_k^P$, the multi-channel Yule-Walker equations specified by Equation (51) are solved using the Levinson-Durbin recursion to determine the matrix coefficients $A_c^H(p)$ and the Hermitian driving white noise covariance matrix $[\Sigma_u]_c^H$ for p = 1, 2, ..., P.

$$A^H R_k^P = \left\{ [\Sigma_u]_c^H \quad [0] \quad \cdots \quad [0] \right\} \tag{75}$$

where

$$A^H = \left[ I \quad A^H(1) \quad A^H(2) \quad \cdots \quad A^H(P) \right] \tag{76}$$

$$[\Sigma_u]_c^H = E\left[ \underline{u}\underline{u}^H \right] = [\Sigma_u]_c \tag{77}$$

$$\underline{u}(n) = \begin{bmatrix} u_1(n) \\ u_2(n) \\ \vdots \\ u_J(n) \end{bmatrix} \tag{78}$$

4. Perform the SVD of the matrix $[\Sigma_u]_c^H$; i.e.,

$$[\Sigma_u]_c^H = USU^H = (US^{1/2})(US^{1/2})^H \tag{79}$$

5. These matrices are now used in the generation of $\underline{\tilde{c}}(n)$ using

$$\underline{\tilde{c}}(n) = -\sum_{p=1}^{P} A_c^H(p)\underline{\tilde{c}}(n-p) + \underline{\tilde{u}}_c(n) \tag{80}$$

where

$$\underline{\tilde{u}}_c(n) = (U_c S_c^{1/2})\underline{\tilde{v}}_c(n) \tag{81}$$

and $\underline{\tilde{v}}_c(n)$ is a white noise vector whose covariance matrix is the identity matrix..

# 6

# Examples

In this section, we give some examples showing how the proposed algorithms perform. Note also that part of this work set the stage for a more sophisticated MATLAB-based tool referred to as the Air Force Research Lab (AFRL) Multi-Channel Signal Processing System (MCSPS). This tool allows the researcher to have a complete radar system analysis, starting with a thorough and detailed signal generation, choice of signal processing technique and diagnostics. It is the first part of the algorithm that we will be using in this section.

To simplify the analysis, the scenario used consists of J = 14 channels and N = 16 pulses. In all examples, additive white Gaussian noise is assumed to be present. Two cases are considered. In addition to the clutter, a target is always present, but no jammer will be present in the first case whereas the second case has a jammer included in the simulation. In all cases, the target is assumed to be located at an azimuth angle of -30° and elevation angle of 0°. Moreover, it is assumed to have a 0.5 normalized Doppler and a Signal to Interference plus Noise ratio (SINR) of 10 dB. In all cases 361 clutter patches are assumed to make up the clutter ring. The parameters used in the simulation will be described for each case. We start with the representative model.

## 6.1. Representative Model

As was described earlier, this model generates data following a very simple covariance matrix formulation. In the following, we plot the angle/Doppler map. The scenario consisted of clutter and a single target. The shaping parameters $\mu_t$ and $\mu_s$ have been varied so as to generate different clutter shapes.

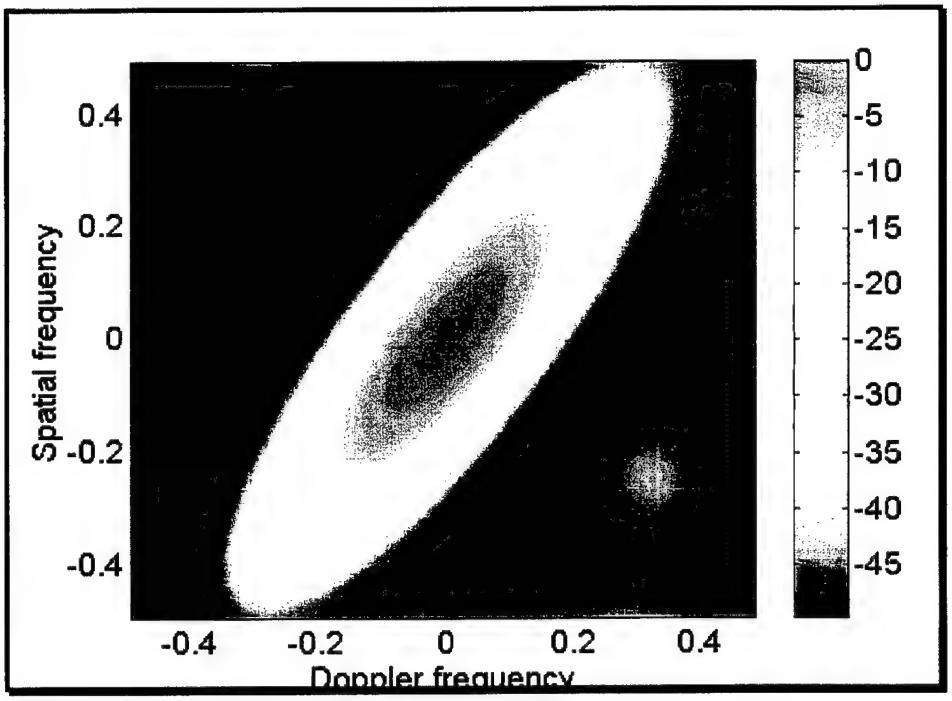


**Figure 9. Angle/Doppler map, $\mu_t = 0.9999$, $\mu_s = 0.75$.**

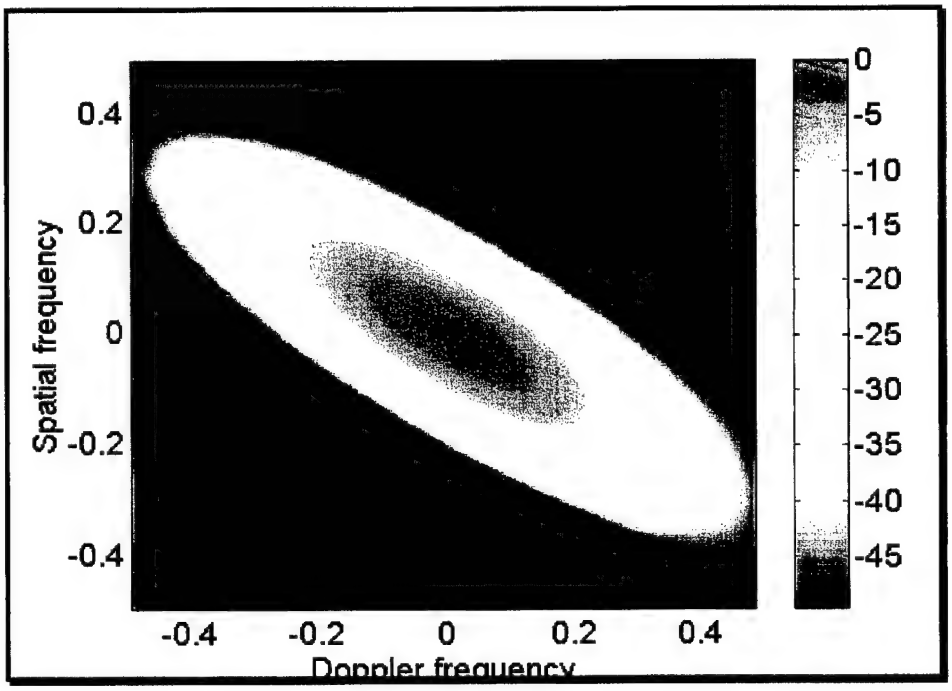


**Figure 10. Angle/Doppler map, $\mu_t = 0.75$, $\mu_s = 0.9999$.**

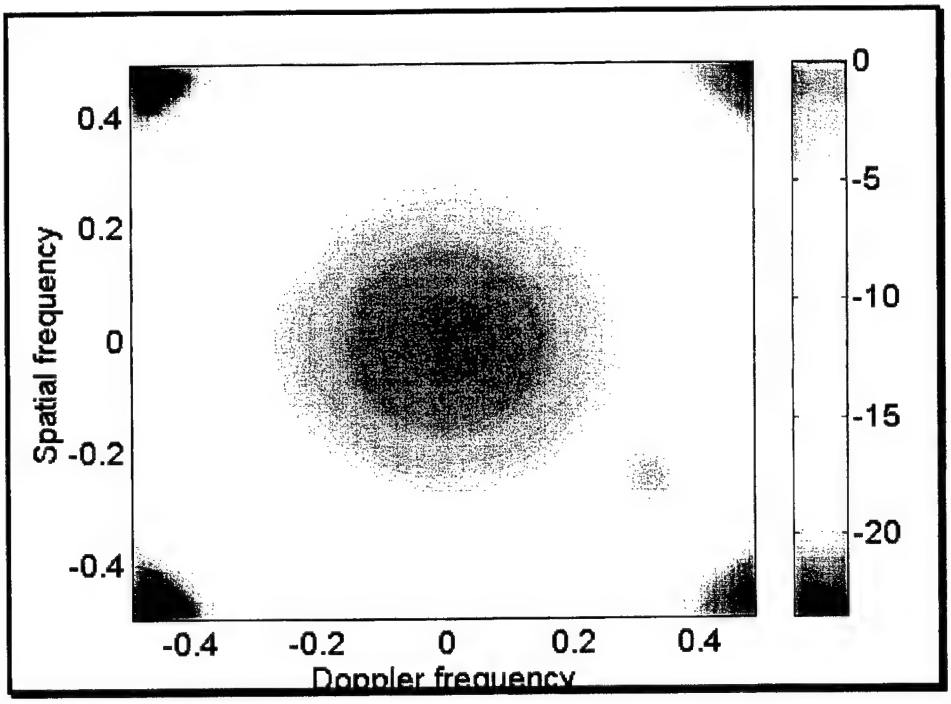


**Figure 11. Angle/Doppler map, $\mu_t = 0.5$, $\mu_s = 0.5$.**

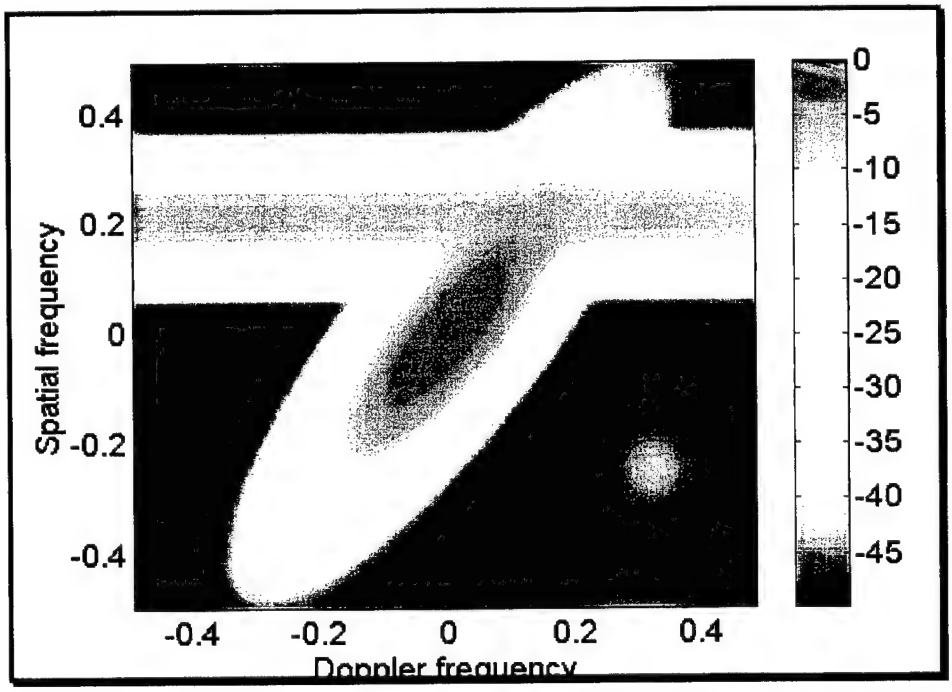


**Figure 12. Angle/Doppler map, $\mu_t = 0.5$, $\mu_s = 0.5$, 1 jammer.**

Figure 9 shows the case of highly correlated clutter (in time), whereas the spatial correlation is moderate. This leads to a narrow clutter beam in the angle/Doppler map. Figure 10 is

similar to figure 9. The values of $\mu_t$ and $\mu_s$ have been switched and therefore, the clutter ridge shows up in the other opposite direction. Since the target remained in the same location (angle and Doppler), whereas it was in the clear in figure 9, it now competes with very strong sidelobe clutter. When the values of $\mu_t$ and $\mu_s$ have been assumed to be similar and equal to 0.5, the resulting clutter spectrum resembles that of a bell (see figure 11). In figure 12, a jammer was added to the interference and shows at all Doppler, with a normalized spatial frequency of 0.2.

## 6.2. Physical Model

The following examples are taken from the physical model.

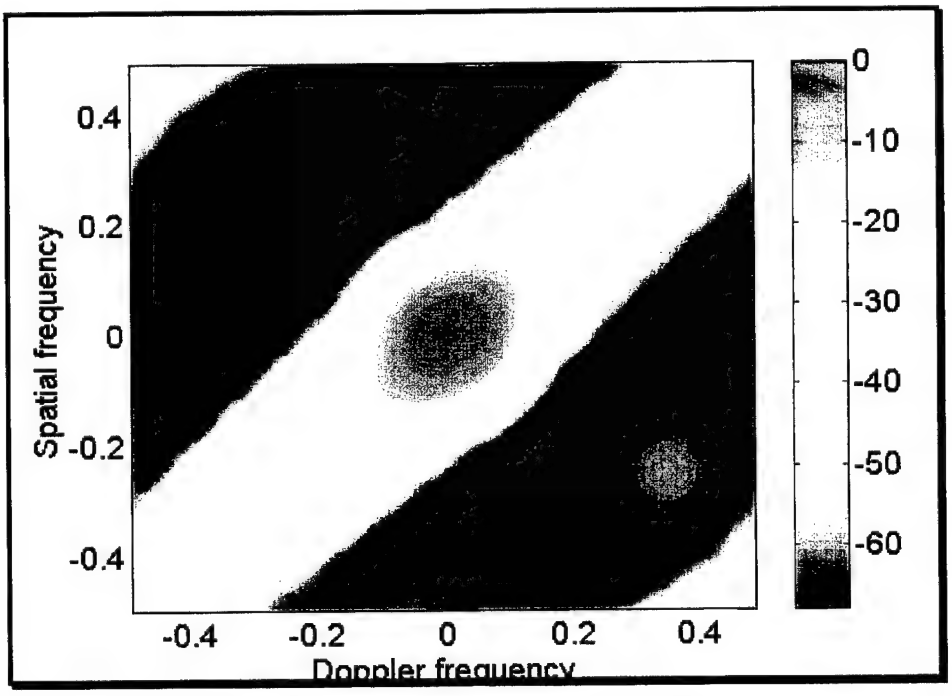


**Figure 13. Angle/Doppler map, $v_p$ = 50.**

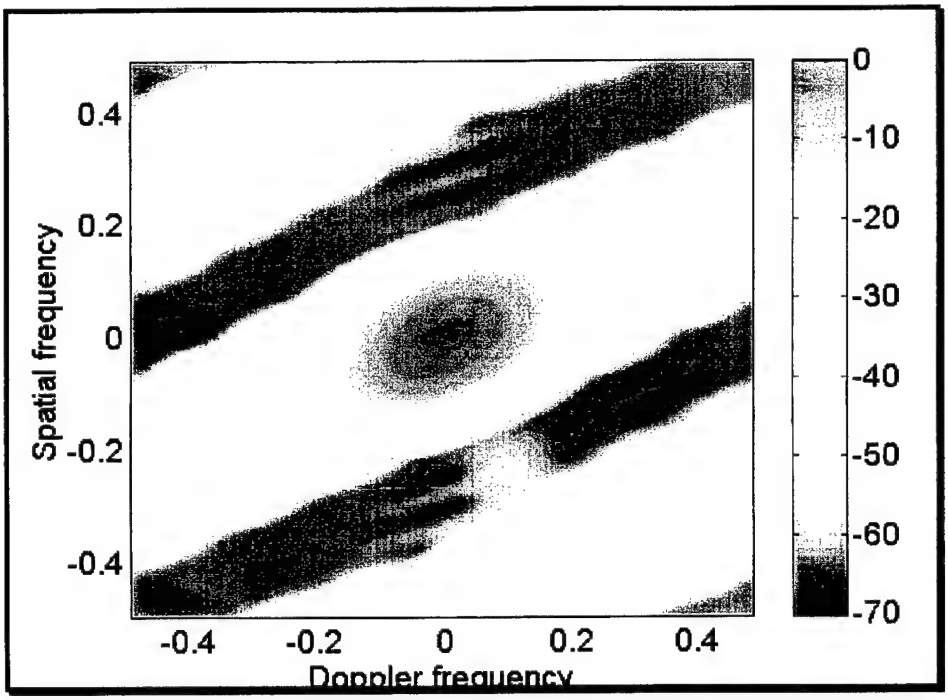


**Figure 14. Angle/Doppler map, $v_p$ = 100.**

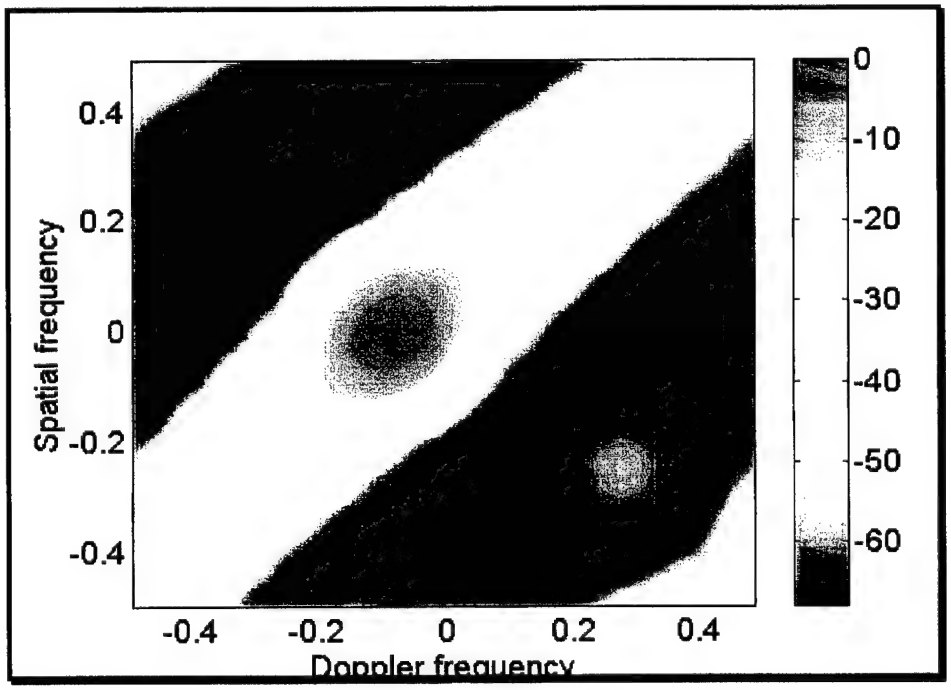


**Figure 15. Angle/Doppler map, $v_p$ = 50, crab angle = 10°.**

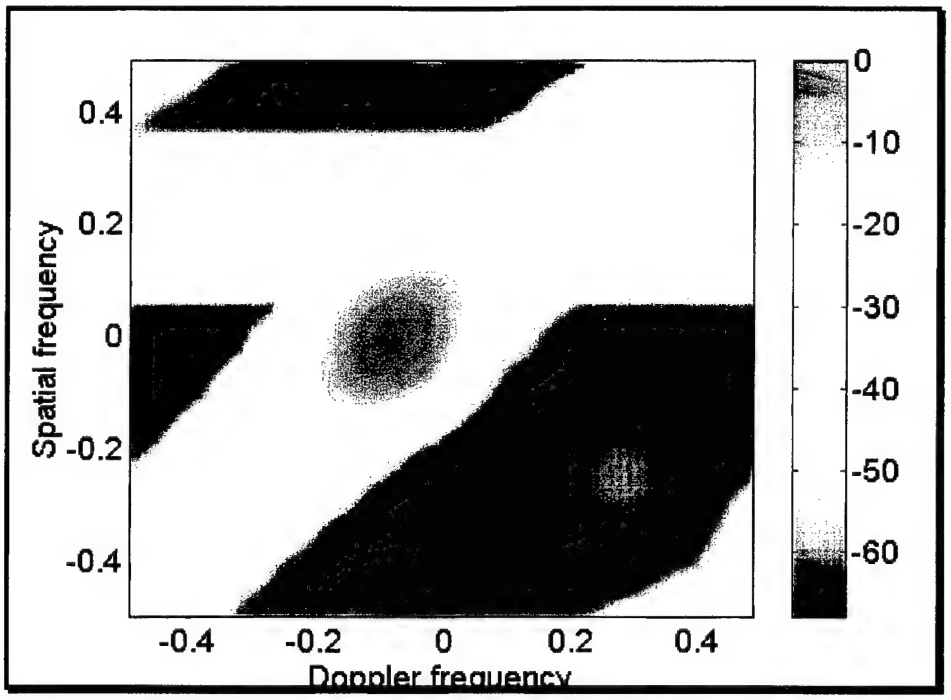


**Figure 16. Angle/Doppler map, $v_p$ = 50, 1 jammer.**

In figure 13, the platform velocity was assumed to be 50 m/s. Along with other parameters, this leads to clutter ridge along the diagonal in the angle/Doppler map. If this speed is doubled (100 m/s), this situation creates ambiguities as can be seen in figure 14. In both cases, the crab angle was assumed to be 0°. Figure 15 shows the case when the crab angle is equal to 10°; this leads to a curved clutter ridge. Again, if a jammer is added to the scenario, it will appear all Dopplers at a specific angle, as is the case in figure 16. The examples shown above are simply an illustration of the way different spectra could be generated.

## 6.2 Hybrid Model

In this section, we present examples taken from the hybrid model. In this case the clutter ridge slope is taken to be and a temporal clutter one lag of 0.9 is also assumed. Figures 17-19 show the spectrum of the described scenario as a function of $\mu_t$.

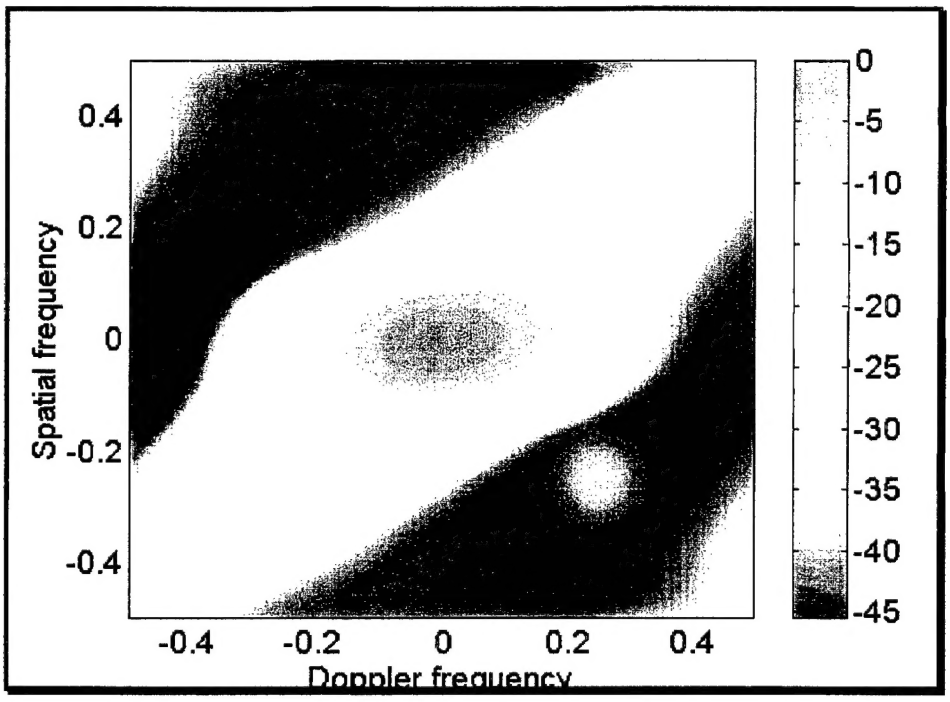


**Figure 17. Angle/Doppler map, $\mu_t = 0.9$.**

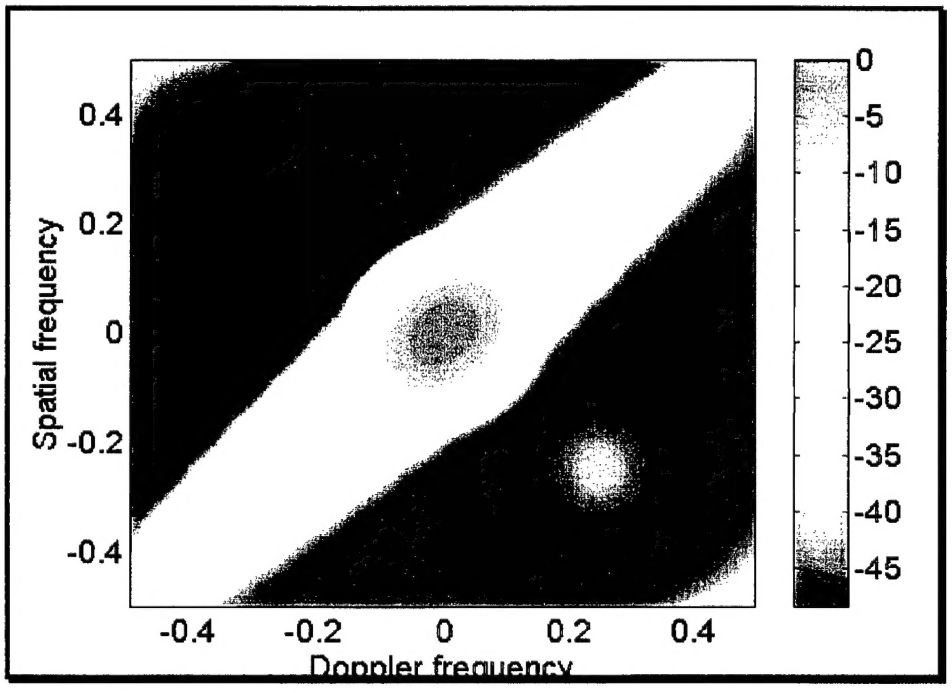


**Figure 18. Angle/Doppler map, $\mu_t = 0.9999$.**

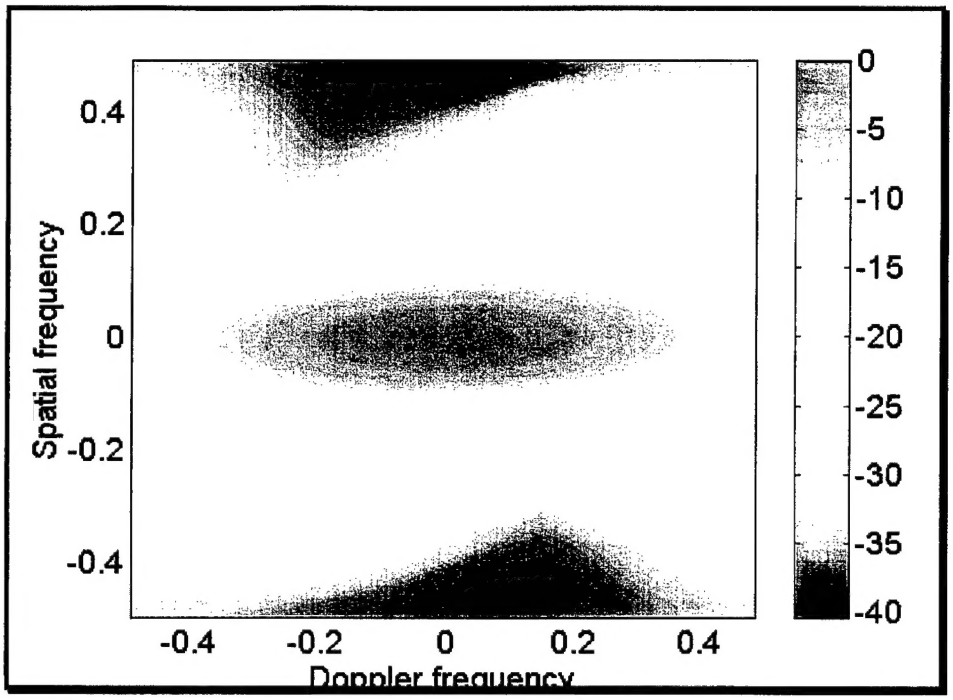


**Figure 19. Angle/Doppler map, $\mu_t = 0.5$.**

# 7
# Conclusions

In this short report, we described three techniques for data generation. These techniques have successfully been implemented into the AFRL-MCSPS simulation and analysis tool. Engineers at AFRL are developing and studying advanced signal processing techniques such as STAP, using this tool. The way data signals are generated and the confidence in the approach used are very essential for a good and thorough performance evaluation. For these reasons, we have decided to include all three techniques as part of the signal generation capability of the tool. In section 6 of the report, we have given example of spectra generated through the tool, using the proposed approaches. We have shown that these spectra are representative of actual airborne data.

Once the covariance matrix has been computed using any of the three proposed techniques, space-time data is generated using a matrix factorization technique. We have tried several techniques such as the Cholesky decomposition, the SVD decomposition, the LDL decomposition, the eigen-decomposition, and the square root of the matrix (MATLAB function). Of all the techniques mentioned above, we found that the SVD performed the best in terms of robustness to numerical inaccuracies as well as speed of execution. We have then decided to implement only this technique for data generation.

Present and future work involves developing more sophisticated target signal and jammer signals. This will be described in future reports.

# *MISSION*
# *OF*
# *AFRL/INFORMATION DIRECTORATE (IF)*

The advancement and application of information systems science and technology for aerospace command and control and its transition to air, space, and ground systems to meet customer needs in the areas of Global Awareness, Dynamic Planning and Execution, and Global Information Exchange is the focus of this AFRL organization. The directorate's areas of investigation include a broad spectrum of information and fusion, communication, collaborative environment and modeling and simulation, defensive information warfare, and intelligent information systems technologies.